Properties comparison of dielectric ceramic parts manufactured by powder pressing and injection molding

Z. Chen[*a], T. Li[a], S. L. Liew[b], S. Wang[b], L. Chen[c]

[a] Singapore Institute of Manufacturing Technology (SIMTech), Agency for Science, Technology and Research (A*STAR), 2 Fusionopolis Way, Singapore 138634, Republic of Singapore

[b] Institute of Materials Research and Engineering (IMRE), Agency for Science, Technology and Research (A*STAR), 2 Fusionopolis Way, Singapore 138634, Republic of Singapore

[c] Dou Yee Technologies Pte. Ltd., 113 Defu Lane 10, Singapore 539227, Republic of Singapore

[*]Corresponding author, email address: chen_zhe@simtech.a-star.edu.sg

Abstract

Dual-phase dielectric ceramic samples of $Mg_2SiO_4/Ba(AlSiO_4)_2$ were fabricated by ceramic injection molding (CIM), and they were systematically compared with the ones fabricated by conventional powder pressing (CP). It was found that by tuning the processing parameters, CIM samples with density, microstructure, grain size, and phase composition comparable with the CP counterparts can be produced. With optimized processing parameters, CIM samples with a relative density of 94.2% were accomplished, along with homogenous phase distribution and uniform grain size. Meanwhile, satisfactory dielectric properties were also achieved (a dielectric constant of 6.67, a temperature coefficient of -0.94 ppm/ºC, and a quality factor of 352,000 GHz). Moreover, a demonstrator with various blind holes and slots was fabricated by the CIM method, which exhibited good geometrical integrity, uniform microstructure, and consistent mechanical properties.

Keywords: dielectric ceramics, properties comparison, powder pressing, ceramic injection molding

1 Introduction

Dielectric ceramics, which are widely employed as filters and resonators in communication equipment, have gained increasing popularity due to the rapid advancement of microwave telecommunication technologies [1-3]. One of the most common techniques for dielectric ceramic parts manufacturing is conventional powder pressing (CP), which allows effective large-scale production, though limited by structure complexity. Respective parts possess desirable dielectric properties, including a low dielectric constant (ε_r) for less signal delay, a high quality factor ($Q \times f$) for adequate signal selectivity, and a near-zero temperature coefficient of resonant frequency (τ_f) for stable utilization under dynamic conditions[4,5]. However, with more novelly designed dielectric ceramic parts emerging, it's challenging for the conventional powder pressing to accommodate a higher demand for complicated geometrical features of these parts, such as varied wall thickness and blind channels.

Ceramic injection molding (CIM) is an advanced ceramic forming technology, which enables efficient production of ceramic parts with high dimensional precision and complex geometrical structures [6,7]. The feedstock for CIM is a homogeneous mixture of ceramic powders and a selected binder system. The mixture, under the effects of heating and shearing stress, is injected into a pre-designed mold, thereby forming ceramic green parts after cooling in the mold. The final parts are realized by following binder removal and sintering steps. Nevertheless, the large proportion of organic matter in CIM feedstock leads to a low parts density after debinding, which raises the defects formation probability during the sintering stage, such as pores and cracks. Additionally, phase separation may occur in microstructure because of the necessary shear stress involved in the CIM process. By adjusting feedstock systems and processing parameters, CIM has been successfully employed in structural ceramics manufacturing, such as Al_2O_3 [8], ZrO_2 [9], Si_3N_4 [10], etc., where homogeneous microstructure, satisfactory density and mechanical properties have been achieved. However, research work on functional ceramics manufacturing by CIM, e.g., dielectric ceramics, is very limited. This is possibly because functional properties of ceramics are more sensitive to micro defects and phase inhomogeneity of ceramics, compared with mechanical ones. For example, cordierite-mullite ceramic parts were fabricated by CIM, and reduced dielectric properties were recorded, due to the variation of phase

formation in a CIM process [11]. Glass ceramics were also processed by CIM for photoluminescence studies, and a rise in structural defect population was detected for CIM samples compared with the conventional powder-pressed counterparts [12]. Single phase microwave dielectric ceramics ($Ba(Zn_{1/3}Ta_{2/3})O_3$) were fabricated by CIM [13], and a significant reduction of density and dielectric properties was observed, compared with powder-pressed samples sintered at the same temperature, which was due to inhomogeneous microstructure, such as a high porosity level caused by binder flow.

The aim of this work is to fabricate dielectric parts, via the CIM method, with complicated structures and comparable dielectric properties to conventional powder-pressed parts, by tuning processing parameters. A dual-phase dielectric ceramic of Mg_2SiO_4 and $Ba(AlSiO_4)_2$ is selected, to study the phase distribution in the CIM process. Effects of processing parameters on density, microstructure, phase composition, and dielectric properties (quality factor, dielectric constant, and temperature coefficient of resonant frequency) are investigated, and the relationship between processing, microstructure, and properties of parts is analyzed. Moreover, a systematic comparison between CP parts and CIM parts manufactured with the same dielectric feedstock is conducted. A demonstrator with various blind holes and through slots is also fabricated to show the capability of CIM for complex structure realization.

2 Experimental

2.1 Materials

The ready-to-press dielectric ceramic powders ($Mg_2SiO_4/Ba(AlSiO_4)_2$) were provided by Boom High Purity Materials Technology Co. Ltd., China, and the chemical composition is listed in Table 1. The inhouse thermoplastic binder formula for the CIM process consisted of polypropylene, paraffin wax, and stearic acid, which were supplied from Sigma-Aldrich Pte. Ltd. in Singapore.

Table 1 Chemical composition of the raw dielectric ceramic

Mg_2SiO_4	$Ba(AlSiO_4)_2$	Original Binder
46.2 wt.%	48.4 wt.%	5.4 wt.%

The dielectric ceramic powders were further characterized, and results indicated the powders were spray dried to form spherical clusters with D50 of 150 μm for a good flowability. Each cluster consisted of irregular prime particles with an average size of 1 μm.

2.2 Processes and Characterizations

For the conventional powder pressing (CP) process, the ready-to-press dielectric ceramic powders were used just as received. Disc-shaped samples were pressed uniaxially under 200 MPa via a manual hydraulic press, with a thickness of 0.8 mm and a diameter of 30 mm.

For the ceramic injection molding (CIM) process, a calcination step, with a holding temperature of 700 ºC for 2 h, was performed on the raw powders, in order to remove the original binder, so that the treated powders could be well dispersed in the inhouse proprietary binder system. CIM feedstock was prepared by homogenizing calcined powders, polypropylene, paraffin wax, and stearic acid in a ROSS double planetary mixer (Model LDM-1QT, US), with a solid loading of 49 vol%. The uniform mixture was cooled, crushed, and ready for a CIM process. A mold for disk-shaped samples was designed and provided by a local mold manufacturing company. The CIM process was conducted with an injection molding machine from Arburg GmbH (Model 220S-15-60, Germany), and the main injection molding parameters are listed in Table 2. The resulting CIM green parts were first debound in isopropyl alcohol at 70 ºC for 12 h, to partially dissolve some components of the binder. The remaining binder was further removed by a following thermal debinding step via a CARBOLITE tube furnace (Model STF15/450, UK), with a maximum holding temperature of 600 ºC. Subsequently, a sintering step was performed on both CP and CIM samples in the same batch to consolidate the powders, by a CM box muffle furnace (Model 1712 FL, US). The holding temperature ranges from 1200 ºC to 1350 ºC, with a dwell time of 4 h.

The density of all sintered samples was collected by the Archimedes method. The microstructure of samples was investigated by a Field Emission Scanning Electronic Microscope (FE-SEM, ZEISS ULTRA plus, Germany). Phase compositions were identified with an X-ray diffraction machine (XRD, Bruker D8 Advance with Cu Kα radiation, 40 kV). The hardness values were recorded with a microhardness tester from MATSUZAWA (Model MMT-X3, Japan). Computed Tomography (CT) scan was performed to check the overall integrity of fabricated samples via a microfocus CT system (Phoenix v|tome|x m, GE, US). The microwave dielectric properties were collected by the Hakki-Coleman dielectric resonator method. A split post dielectric resonator was connected to a vector network analyzer

(10MHz – 24GHz, ZVA 24, Rohde & Schwarz GmbH, Germany) to measure the quality factor (Q×f), dielectric constant and resonant frequency in the temperature range of 23 ºC to 80 ºC, based on which the temperature coefficient of resonant frequency (τ_f) was calculated from the equation,

$$\tau_f = \frac{f_{80} - f_{23}}{f_{23}(80 - 23)}$$

where f_{80} and f_{23} denote frequencies at 80 ºC and 23 ºC, respectively.

Table 2 Main processing parameters of CIM

Injection speed (ccm/s) Step 1; step 2; step 3	12; 15; 10
Holding pressure (bar)	500
Barrel temperature (ºC) Nozzle; front; middle; rear	163; 160; 155; 148
Cooling Time (s)	10
Dosage volume (ccm)	8

3 Results and Discussion

3.1 Effects of ramping rate in the thermal debinding stage

CIM green parts are featured with a high proportion of organic components, and therefore the binder removal process in the thermal debinding stage influences defects forming probability directly, thereby impacting quality of sintered dielectric parts. The holding temperatures at different steps of the thermal debinding stage are determined by the decomposition temperatures of organic components in CIM feedstock. According to the adopted inhouse proprietary binder system, temperature-holding steps in this work were fixed at 240 ºC, 360 ºC, 480 ºC, and 600 ºC, with a dwell time of 2 h at each step, while the ramping rate of the whole thermal debinding stage was varied from 0.5 ºC/min to 5 ºC/min to study its effects on sintered parts. Fig.1 shows the relative density of dielectric samples sintered at 1250 ºC, with different ramping rates in the thermal debinding stage. A significant reduction of density can be observed from 92.5% to 86.0%, when raising the ramping rate from 0.5 ºC/min to 5 ºC/min.

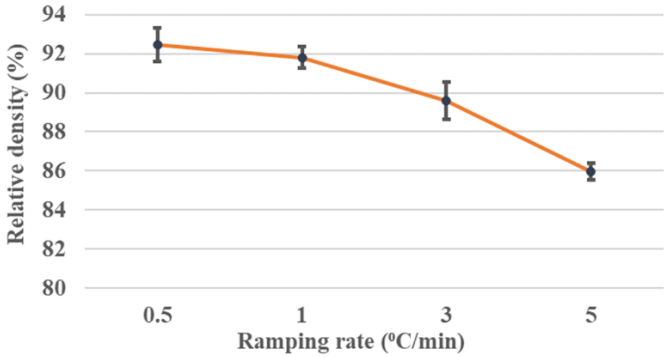

Fig. 1 Relative density of CIM samples vs. ramping rate in the thermal debinding stage

SEM images of these samples at different magnifications are presented in Fig. 2. As can be seen from images of lower magnification (Fig. 2a-d), the surface of samples transits from flat to wavy state. When the ramping rate reaches 5 ºC/min, small blisters and holes can be observed, owing to the escaped gas from organic matter decomposition. After the solvent debinding process, some of the organic matter was dissolved in IPA and left small holes and channels in dielectric samples, which acted as gas escaping paths for the following thermal debinding process. Smooth gas escaping takes place when the gas escaping rate is slow, resulted from a lower ramping rate of the thermal debinding process. Consequently, the respective samples' surface looks flat. In contrast, if the ramping rate is too high, the pores/channels formed in the solvent debinding stage cannot accommodate high-volume gas escaping in a short time, which exerts increasing stress on the green bodies, causes wavy surface, and even leads to blisters and holes at surface.

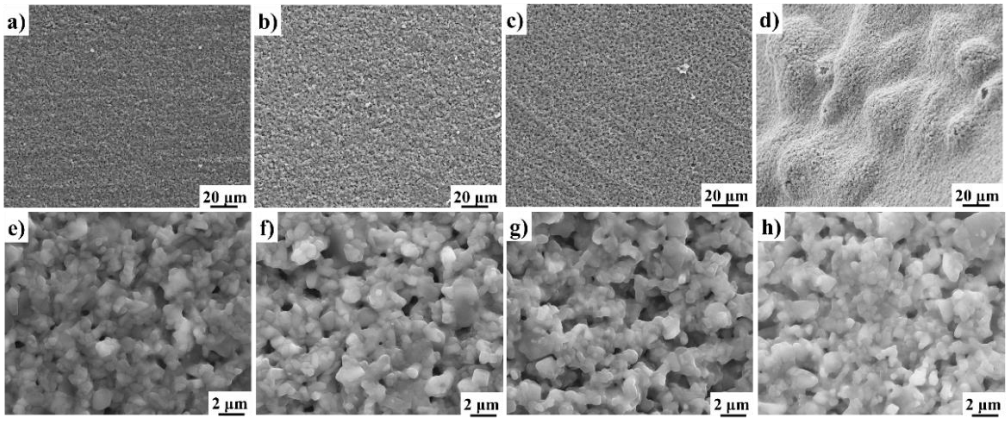

Fig. 2 SEM images under different ramping rates: Low magnification, a) 0.5 ºC/min, b) 1 ºC/min, c)3 ºC/min, d) 5 ºC/min; High magnification, e) 0.5 ºC/min, f) 1 ºC/min, g) 3 ºC/min, h) 5 ºC/min

Fig. 2e-g illustrates the high-magnification SEM images of samples with a ramping rate from 0.5 ºC/min to 3 ºC/min. Expanding pore size can be detected, which is caused by the increasing gas escaping rate. These micro-scale pores indicate an impeded powder consolidation process during the sintering stage and result in a reduced density of samples. When the ramping rate was 5 ºC/min, the quickly escaped gas caused uneven microstructure, where blisters and holes formed at certain areas on the surface and released internal stress, while dense microstructure with small pores dominated in other areas, as is shown in Fig. 2h. These results reveal that it is necessary to tune the ramping rate to a proper level to allow a mild gas escaping process in the debinding stage, which plays a key role in reducing defects forming probability in the following sintering stage. In this work, a ramping rate of 1 ºC/min is adopted to balance the quality of samples and processing efficiency. The respective samples possess higher final density and homogeneous microstructure, compared with counterparts with faster ramping rates, meanwhile, the thermal debinding process is less time-consuming than the situation with the lower ramping rate of 0.5 ºC/min.

3.2 Effects of holding temperature in the sintering stage

Holding temperature is one of the most influential factors in the sintering stage, which impacts atom diffusion, phase forming, homogeneity of microstructure, and final density of ceramic parts. In this work, sintered CP samples and CIM samples were produced simultaneously within a holding temperature range of 1200 ºC and 1350 ºC, to have a decent comparison of samples by two different processing methods. Fig. 3 shows the density variation of both CP and CIM samples versus the holding temperature. As can be expected, the density of CP samples is higher than the CIM ones in the whole range of holding temperature, because of a much higher proportion of organic matter in CIM feedstock which causes a lower packing density of powders after thermal debinding. At the same time, the density variation trends for both sets of samples are the same, rising with increasing holding temperature, peaking at 1300 ºC, and then dropping when holding temperature is further raised to 1350 ºC.

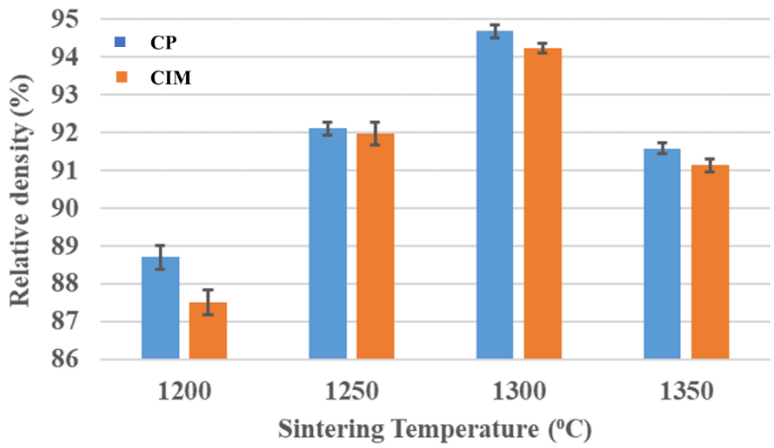

Fig. 3 Density variation of CP and CIM samples vs. sintering temperature

SEM images of samples' microstructure are collected to analyze this density variation trend. As can be seen from Fig. 4, the microstructure of both CP and CIM samples is characterized by dual phases (bright and dark area) and irregular pores. The pore size at 1150 ºC is about 1 μm, and the porosity level is remarkably reduced with increasing holding temperature, owing to the enhanced atoms diffusion, which explains rising density values from 1200 ºC to 1300 ºC. The microstructure of the CIM sample is comparable to the CP one, with a homogeneous distribution of two phases and a very limited porosity level, when the holding temperature reaches 1300 ºC. This reveals that the shearing stress in the injection molding process did not cause undesirable phase separation effects. However, when further raising the sintering temperature to 1350 ºC, large and regular-shaped pores occur in both CP and CIM samples as is shown in Fig. 4d and 4h, with an average pore size of 8.7 μm, which leads to a sharp decline in the density of samples.

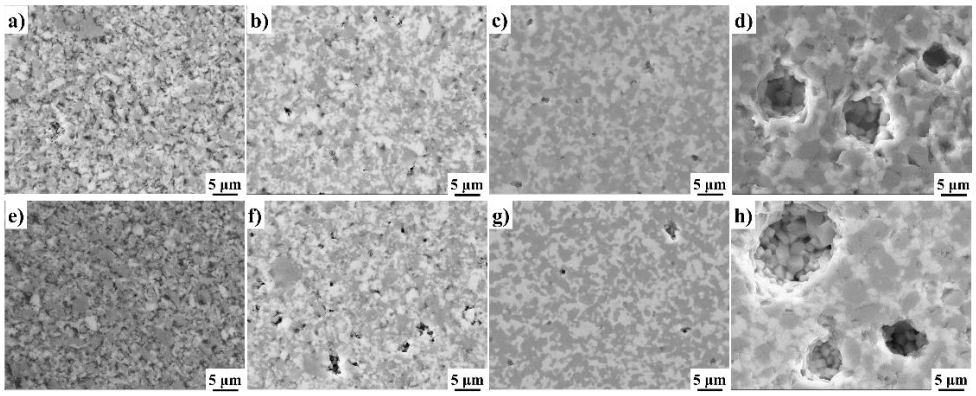

Fig. 4 SEM images of CP and CIM samples sintered at different temperatures: a) CP 1200 ºC, b) CP 1250 ºC, c) CP 1300 ºC, d) CP 1350 ºC, e) CIM 1200 ºC, f) CIM 1250 ºC, g) CIM 1300 ºC, h) CIM 1350 ºC

To identify the root cause, XRD patterns were further recorded and analyzed, as can be seen in Fig. 5 and Fig. 6. When the holding temperature ranges from 1250 ºC to 1300 ºC, both CP and CIM samples consist of 3 phases, as indicated by the positions of peaks. Apart from major phases of $Ba(AlSiO_4)_2$ and Mg_2SiO_4, $MgSiO_3$ occurs as an additionally minor phase, which is commonly formed from Mg_2SiO_4 in a heat treatment process, either due to partial decomposition of Mg_2SiO_4 [14,15], or the reaction between Mg_2SiO_4 and remnant amorphous SiO_2 in raw materials [16]. Nonetheless, such $MgSiO_3$ by-product is converted to Mg_2SiO_4 again when the holding temperature is raised to 1350 ºC, as can be seen from Fig. 5d and 6d, where no peak corresponding to $MgSiO_3$ is recorded.

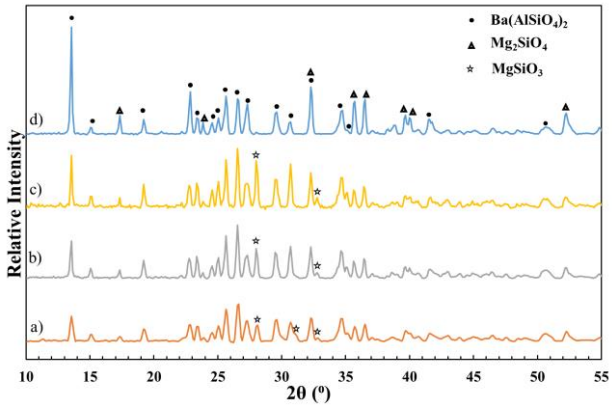

Fig. 5 XRD patterns of CP samples sintered at different temperatures: a) 1200 ºC, b) 1250 ºC, c) 1300 ºC, d) 1350 ºC

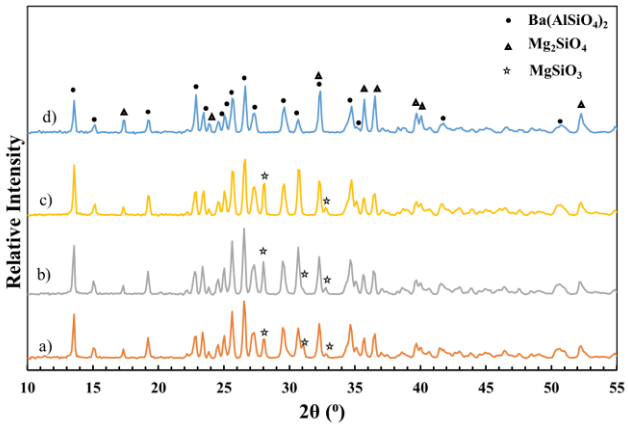

Fig. 6 XRD patterns of CIM samples sintered at different temperatures: a) 1200 ºC, b) 1250 ºC, c) 1300 ºC, d) 1350 ºC

A possible chemical reaction is suggested as follows,

$$2MgSiO_3 \leftrightarrow Mg_2SiO_4+SiO_2$$

which is similar to some proposed reactions in previous literature works [16-19]. Since SiO_2 peaks are not detected from XRD patterns, it is believed the resulting SiO_2-rich liquid phase from dissociated $MgSiO_3$ evaporated in the sintering process, which caused the presence of large pores on samples sintered at 1350 ºC. Additionally, one common concern for the CIM process is that the remnant organic matter may react with ceramic powders at a high temperature and form certain impurity phases. TGA results of CIM feedstock (Fig.S1, Supplemental Information) indicated that the additional binder fully decomposed at temperature higher than 600ºC, and no products of reaction between ceramic phase and binder were detected by XRD.

The effects of holding temperature on grain size are also studied by collecting SEM images of unpolished samples sintered at different temperatures, as can be seen in Fig. 7. At the same temperature level, the grain size and morphology of CP and CIM samples are comparable, and an evident grain growth is well observed with an increasing holding temperature. The statistical data on grain size of two types of samples is listed in Table 3. For CP samples, the average grain size rises from 0.76 μm to 2.88 μm, when raising the holding temperature from 1200 ºC to 1350 ºC, and from 0.73 μm to 3.17 μm for CIM samples. It can be seen that the grains of Mg_2SiO_4 and $Ba(AlSiO_4)_2$ are bonded densely with a homogeneous distribution at a higher sintering temperature, which again confirms that no phase separation occurs under the effects of shear stress in CIM. Based on the aforementioned results, a holding temperature of 1300 ºC is selected to achieve a dense microstructure of sintered dielectric samples, as the relative density of CIM samples is very close to the CP samples (94.2% vs. 94.7%).

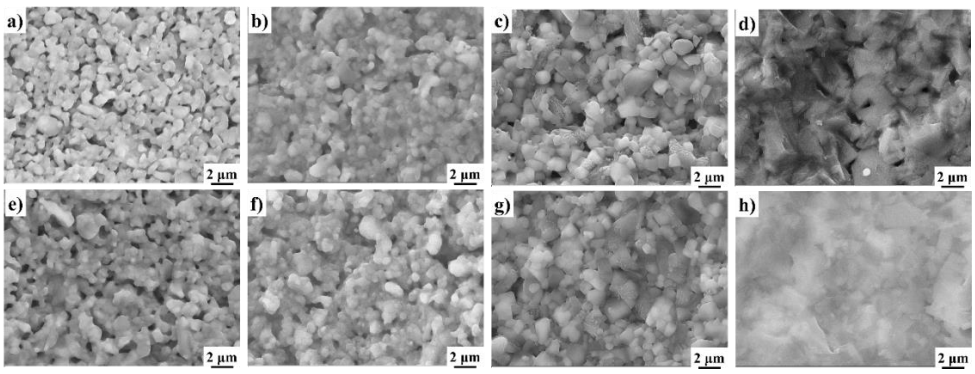

Fig. 7 SEM images of unpolished CP and CIM samples sintered at different temperatures: a) CP 1200 ºC, b) CP 1250 ºC, c) CP 1300 ºC, d) CP 1350 ºC, e) CIM 1200 ºC, f) CIM 1250 ºC, g) CIM 1300 ºC, h) CIM 1350 ºC

Table 3 Statistical data on grain size of CP and CIM samples

Sintering Temperature (ºC)	CP samples (μm)	CIM samples (μm)
1200	0.76 ± 0.01	0.73 ± 0.02
1250	0.86 ± 0.07	0.90 ± 0.22
1300	1.24 ± 0.27	1.37 ± 0.14
1350	2.88 ± 0.66	3.17 ± 0.20

3.3 Dielectric properties

Dielectric properties of CP and CIM samples vs. different sintering temperatures were measured and illustrated in Fig. 8. For the dielectric constant (Fig. 8a), it is primarily influenced by the porosity level of parts, and several models have been established to fit the correlation between dielectric constants and porosity of dielectric ceramics [20-22]. These fitting results indicate an approximately negative linear correlation between dielectric constants and porosity level, which explains the same variation trend of dielectric constants as the one of density (Fig. 3), regarding different sintering temperatures. Furthermore, the dielectric constant difference is very small between CP and CIM samples sintered at the same temperature, which is caused by the slight relative density differentiation, as indicated in Fig. 3. It is also noteworthy that the dielectric constants of both samples are smaller than 10, which meets the general requirements of dielectric parts to shorten signal delay.

The quality factor (Q×f) of dielectric ceramic samples as a function of sintering temperature is illustrated in Fig. 8b. As results indicate, for both CP and CIM samples, the quality factor raises with increasing temperature, peaks (> 250,000 GHz) at 1300 ºC, and then drops sharply below 100,000 GHz when the sintering temperature reaches 1350 ºC. Compared with the dielectric constant, the quality factor is a more complex quantity, which is impacted by many factors, such as porosity, grain size, lattice flaws, etc. Previous literature works reveal that the quality factor declines exponentially with rising porosity levels in dielectric samples [20]. Additionally, it is also observed that the quality factor increases with larger grain size, due to a reduced number of grain boundaries per unit volume [20, 23].

With sintering temperature ranging from 1200 ºC to 1300 ºC, both densifying microstructure and grain growth can be observed, as shown in Fig. 4 and Fig. 7, which means combined effects of porosity and grain size are exerted on the samples, and therefore the quality factor variation with respect to sintering

temperature is much stronger. At 1300 ºC, the dielectric samples are featured with denser microstructure and the average grain size rises from 0.73 μm to 1.37 μm for the CIM samples, and from 0.76 μm to 1.24 μm for the CP samples. Consequently, the maximum quality factor is achieved for both CP and CIM samples. However, when further increasing sintering temperature to 1350 ºC, density drops sharply because of phase transformation and evaporation, which causes a noticeable fall in quality factor. It is worth mentioning that the porosity level of samples sintered at 1250 ºC and 1350 ºC are comparable, but the quality factor of the former is much larger (~100,000 GHz vs. ~50,000 GHz). This is because the pore size features are different for these samples. According to Fig. 4, the pore size of samples sintered at 1350 ºC is about 10 times larger than the ones of 1250 ºC samples, which means the overall free surface area of pores of 1350 ºC samples is much smaller. Previous works indicate that the presence of a free surface leads to a relaxation of the crystal lattice, which enhances the quality factor [20, 23-25]. Therefore, the quality factor of the 1250 ºC sample is larger than the one of the 1350 ºC sample, though the porosity level is close.

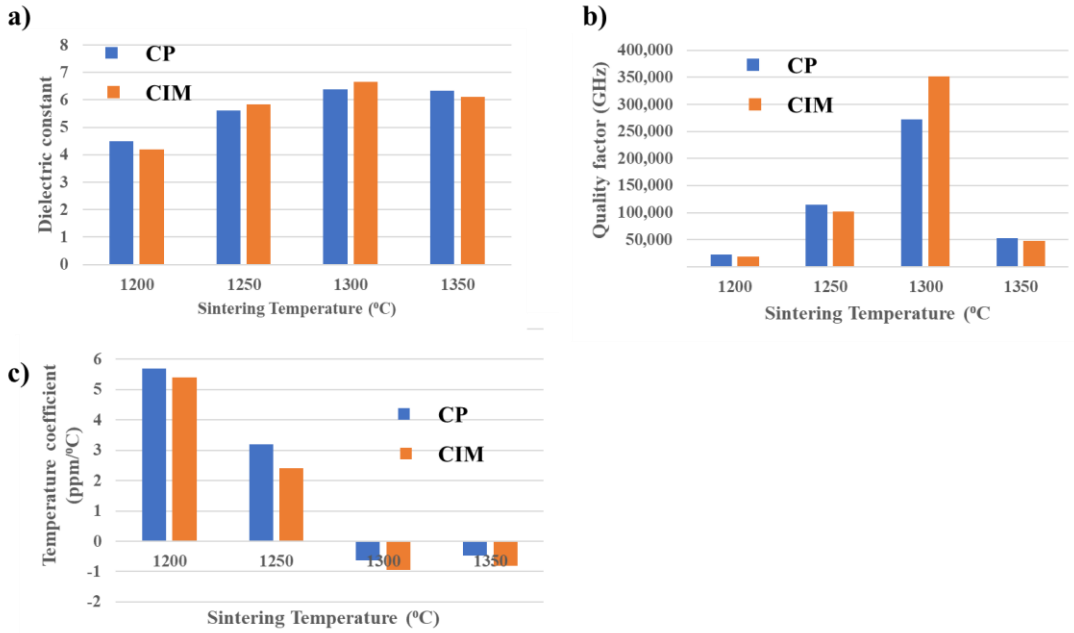

Fig. 8 Dielectric properties of CP and CIM samples vs. different sintering temperatures: a) dielectric constant, b) quality factor, c) temperature coefficient

When comparing the quality factor of CP and CIM samples sintered at the sample temperature, the values are comparable due to similar porosity level and grain size of samples by the two processes, except for the situation at 1300 ºC, where the CIM sample outperforms the CP sample (352,000 GHz

vs. 272,000 GHz). This is possibly because of the grain-scale differences between the CIM and CP samples sintered at this temperature. Although CIM dielectric samples with high quality factors have been accomplished by adjusting the parameters appropriately, further experiments and characterization work would be required to identify the root cause of property differences between CP and CIM samples.

Fig. 8c shows the variation trend of temperature coefficient of resonant frequency versus sintering temperature. Different from the variation trend of dielectric constant and quality factor, it shows that the absolute value of temperature coefficient is monotonously declining with increasing sintering temperature, which is similar to some previously reported literature [26]. For the dual-phase dielectric ceramic in this work, τ_f of Mg_2SiO_4 is negative [27], while τ_f of $Ba(AlSiO_4)_2$ is positive [28]. The overall temperature coefficient of resonant frequency can be close to zero, provided that the grains of two phases are homogeneously distributed and well bonded. When the sintering temperature is lower, atom diffusion of dielectric ceramic samples is not sufficient and grains of two phases are weakly bonded. Consequently, the complementary effect of two phases on τ_f is not significant, and the τ_f value is larger. In contrast, higher sintering temperature leads to dense microstructure and reliably bonded grains, where the complementary grain expansion and contraction from two phases take effect under temperature-changing conditions. Hence the overall temperature coefficient is smaller. A comparison of temperature coefficients between CP and CIM samples reveals that τ_f is not sensitive to different forming processes, so that the coefficients of two types of samples at the same sintering temperature are very close. Specifically, when the sintering temperature is 1300 ºC, the τ_f of CIM sample reaches -0.94 ppm/ºC, which can meet the general requirement for stable utilization of dielectric ceramic parts.

3.4 Demonstrators via the CIM process

Fig. 9 shows a demonstrator of a microwave filter fabricated by the ceramic injection molding process, which is featured with several blind holes and through slots. A weld line can be observed on the green body as is shown in Fig. 9a, which is a junction formed by the convergence of different flow fronts during CIM, and it is commonly found around obstructions in complex molds. After sintering, the weld line disappears due to the effective bonding of particles in the junction area, as can be seen from Fig. 9b. The cross-section images of the sintered demonstrator by CT scanning further confirm that the

junction area is well merged, and no cracks or porosities are detected in the original weld line area. Additionally, it can be seen that the blind hole and slot features are characterized by satisfactory geometrical integrity after sintering.

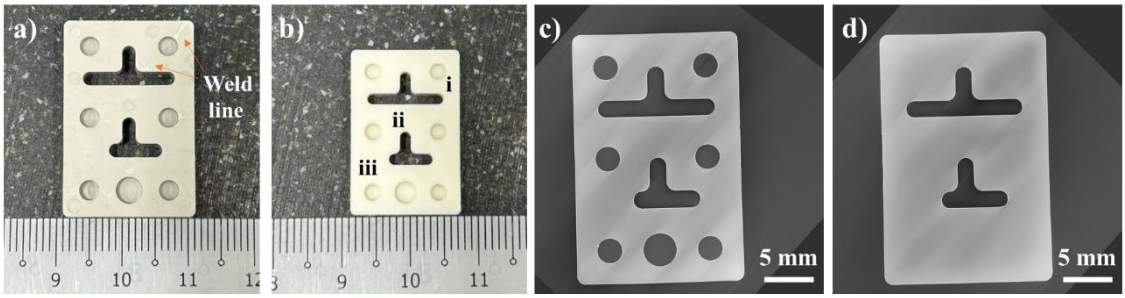

Fig. 9 A demonstrator by CIM method: a) green body, b) sintered body, c) and d) CT scan images at different cross-section

Moreover, cross-section microstructure and hardness are also evaluated to check the homogeneity of CIM dielectric sample. Fig. 10 presents the SEM images of the microstructure at different locations as per Fig. 9b, which indicates a homogeneous microstructure is achieved in the dielectric sample by CIM. In particular, no noticeable defect is detected in the weld line area, and the distribution of two phases is also uniform. Microhardness results are illustrated in Fig. 11, which further reveals a consistent mechanical response of the sample at different locations.

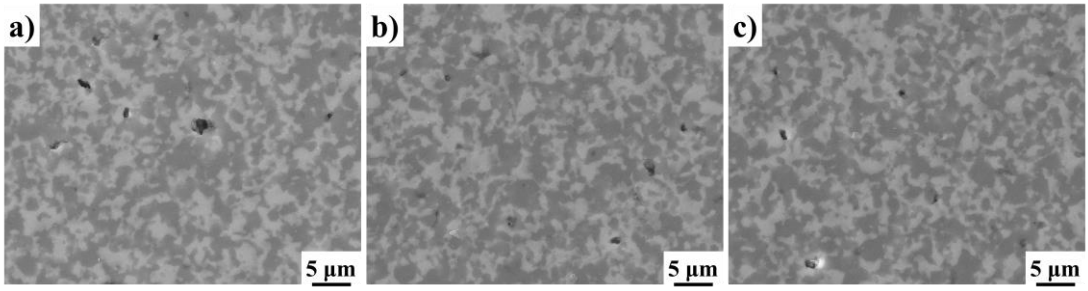

Fig. 10 SEM images of the CIM demonstrator at different locations: a) location i, b) location ii, c) location iii

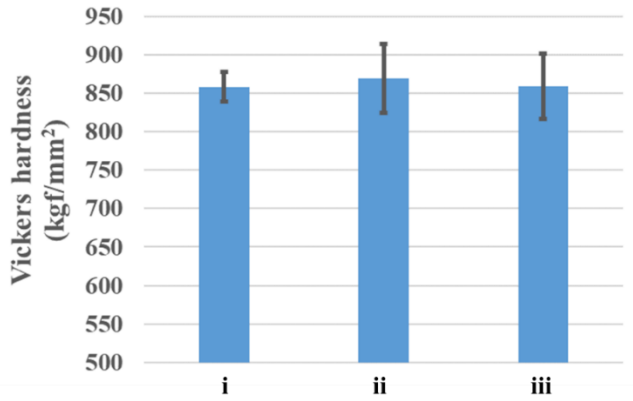

Fig. 11 Microhardness of the CIM demonstrator at different locations

Conclusions

Dual-phase dielectric ceramic samples produced by CIM were compared with the ones by CP, which is considered as the conventional benchmark for ceramic processing. By tuning the processing parameters properly, CIM samples with density, microstructure, grain size, and phase compositions comparable with CP samples can be produced. It is found that the ramping rate of the thermal debinding stage for CIM sample should be sufficiently slow to allow a mild binder removal process which directly impacts defects forming tendency in the following sintering stage. With a ramping rate of 1 ºC/min and a sintering temperature of 1300 ºC, CIM samples with a relative density of 94.2% can be fabricated, along with homogenous phase distribution and uniform grain size.

In this work, the shear stress applied to feedstock in a CIM process does not exert negative effects on dielectric samples, such as phase separation, and no correlation between shear stress and defects forming tendency is identified. Furthermore, when applying optimized processing parameters, the dielectric properties of CIM samples are also comparable to the counterparts by the CP method, achieving a low dielectric constant of 6.67, a near-zero temperature coefficient of -0.94 ppm/ºC, and a high quality factor of 352,000 GHz.

Demonstrators of a microwave filter with various blind holes and slots have also been fabricated by the CIM method, possessing excellent geometrical integrity, uniform microstructure, and consistent mechanical properties, which show that CIM is a promising method for geometrically complex dielectric ceramic parts manufacturing while maintaining the required properties simultaneously.

Acknowledgements

This work is financially supported by the Industry Alignment Fund - Industry Collaboration Project (I2101E0005) from Agency for Science, Technology and Research (A*STAR).

References

[1] Kui, Jiujun. "Microwave dielectric ceramic materials and their industry development overview and future prospects." Journal of Physics: Conference Series. Vol. 1885. No. 3. IOP Publishing, 2021.

[2] Kamutzki, Franz, et al. "Silicate dielectric ceramics for millimetre wave applications." Journal of the European Ceramic Society 41.7 (2021): 3879-3894.

[3] Muccillo, Reginaldo, et al. "Ceramic compositions for 5G devices containing niobium: A survey." International Journal of Ceramic Engineering & Science (2024): e10201.

[4] Lai, Yuanming, et al. "Phase composition, crystal structure and microwave dielectric properties of $Mg_{2-x}Cu_xSiO_4$ ceramics." Journal of the European Ceramic Society 38.4 (2018): 1508-1516.

[5] Ullah, Atta, et al. "Effect of Zn substitution on the sintering temperature and microwave dielectric properties of $MgSiO_3$-based ceramics." Ceramics International 43.1 (2017): 484-490.

[6] Sommer, F., et al. "Injection molding of ceramic cutting tools for wood-based materials." Journal of the European Ceramic Society 33.15-16 (2013): 3115-3122.

[7] Tosello, Guido, et al. "Comprehensive characterization and material modeling for ceramic injection molding simulation performance validations." The International Journal of Advanced Manufacturing Technology 102 (2019): 225-240.

[8] Ani, Sarizal Md, et al. "Fabrication of zirconia-toughened alumina parts by powder injection molding process: Optimized processing parameters." Ceramics International 40.1 (2014): 273-280.

[9] Foudzi, Farhana Mohd, et al. "Yttria stabilized zirconia formed by micro ceramic injection molding: Rheological properties and debinding effects on the sintered part." Ceramics International 39.3 (2013): 2665-2674.

[10] Rueschhoff, Lisa M., et al. "Near-net shaping of silicon nitride via aqueous room-temperature injection molding and pressureless sintering." Ceramics International 43.14 (2017): 10791-10798.

[11] Fuertes, V., et al. "Tailoring dielectric properties of cordierite-mullite ceramics through Ceramic Injection Moulding." Materials Science and Engineering: B 262 (2020): 114783.

[12] Enríquez, E., et al. "Ceramic injection moulding of engineered glass-ceramics: Boosting the rare-earth free photoluminescence." Ceramics International 46.7 (2020): 9334-9341.

[13] Liu, Shaojun, et al. "Structural, chemical and dielectric properties of ceramic injection moulded $Ba(Zn_{1/3}Ta_{2/3})O_3$ microwave dielectric ceramics." Journal of the European Ceramic Society 26.15 (2006): 3273-3278.

[14] Cheng, Lin, et al. "Fabrication of nanopowders by high energy ball milling and low temperature sintering of Mg_2SiO_4 microwave dielectrics." Journal of Alloys and Compounds 513 (2012): 373-377.

[15] Song, K. X., et al. "Effects of Mg/Si ratio on microwave dielectric characteristics of forsterite ceramics." Journal of the American Ceramic Society 90.6 (2007): 1808-1811.

[16] Song, Myung-Eun, et al. "Synthesis and microwave dielectric properties of $MgSiO_3$ ceramics." Journal of the American Ceramic Society 91.8 (2008): 2747-2750.

[17] Wang, W. B., et al. "The synthesis and properties of high-quality forsterite ceramics using desert drift sands to replace traditional raw materials." Journal of the Ceramic Society of Japan 125.3 (2017): 88-94.

[18] Mitchell, Matthew BD, et al. "Preparation of forsterite (Mg_2SiO_4) powders via an aqueous route using magnesium salts and silicon tetrachloride ($SiCl_4$)." Journal of sol-gel science and technology 15 (1999): 211-219.
[19] Chin, KL Jeffrey, et al. "Sintering and properties of magnesium orthosilicate ceramic." Ceramics International 41.10 (2015): 13614-13623.
[20] Penn, Stuart J., et al. "Effect of porosity and grain size on the microwave dielectric properties of sintered alumina." Journal of the American Ceramic Society 80.7 (1997): 1885-1888.
[21] Heidinger, R., and S. Nazare. "Influence of porosity on the dielectric properties of AlN in the range of 30-40 GHz." Powder Metallurgy International 20.6 (1988).
[22] Kingery, W. David, et al. "Introduction to ceramics. " Vol. 17. John wiley & sons, 1976.
[23] Armaki, Hamid Taghipour, et al. "Phase analysis and improvement of quality factor of $Li_2ZnTi_3O_8$ ceramics by annealing treatment." Journal of Alloys and Compounds 581 (2013): 757-761.
[24] Mackrodt, W. C. "The calculated equilibrium segregation of Fe^{3+}, Y^{3+}, and La^{3+} at the low-index surfaces of alpha-Al_2O_3." American Ceramic Society, Inc., Nonstoichiometric Compounds. Advances in Ceramics. 23 (1987): 293-306.
[25] Mackrodt, W. C., et al. "The morphology of α-Al_2O_3 and α-Fe_2O_3: the importance of surface relaxation." Journal of Crystal Growth 80.2 (1987): 441-446.
[26] Liu, Hongxue, et al. "Structural, dielectric, and optical properties of Ni-doped barium cadmium tantalate ceramics." Japanese Journal of Applied Physics 45.12R (2006): 9140.
[27] Lai, Yuanming, et al. "Correlation between structure and microwave dielectric properties of low-temperature-fired Mg_2SiO_4 ceramics." Materials Research Bulletin 99 (2018): 496-502.
[28] Yang, Xiaojing, et al. "Structure and dielectric properties of Ca doped $BaAl_2Si_2O_8$." Ceramics International 44 (2018): S43-S45.